Journal of Drug Delivery Science and Technology 85 (2023) 104584

Contents lists available at ScienceDirect

Journal of Drug Delivery Science and Technology

journal homepage: www.elsevier.com/locate/jddst

Orally fast-dissolving drug delivery systems for pediatrics: Nanofibrous oral strips from isoniazid/cyclodextrin inclusion complexes

Spoorthi Patil [a,1], Asli Celebioglu [b,*,1], Tamer Uyar [b,**]

[a] Biomedical Engineering, College of Engineering, Cornell University, Ithaca, NY, 14853, USA
[b] Fiber Science Program, Department of Human Centered Design, College of Human Ecology, Cornell University, Ithaca, NY, 14853, USA

ARTICLE INFO

Keywords:
Isoniazid
Cyclodextrin
Nanofibers
Fast-dissolving drug delivery system
Oral drug delivery
Pediatric treatment

ABSTRACT

Isoniazid (INH) is an essential antibiotic for tuberculosis that suffers from low water-solubility and limited bioavailability due to its crystalline form. Generation of inclusion complex nanofibrous film of isoniazid with highly water soluble cyclodextrin derivates can enable the development of a new oral delivery system with fast-disintegrating feature. In this study, the inclusion complex (IC) of INH and hydroxypropyl-beta cyclodextrin (HPβCyD) were fabricated into nanofibrous film through electrospinning technique. Here, HPβCyD was used for both encapsulation of INH and electrospinning of free-standing nanofibrous films. Electrospinning of INH/HPβCyD-IC system resulted into uniform and homogenous fiber morphology having ~400 nm mean diameter. The ultimate INH/HPβCyD-IC nanofibers were obtained with a ~100% of loading efficiency (~8% (w/w) of INH content) without loss of drug content during whole process. Due to inclusion complexation, the electrospinning and amorphization of INH within the INH/HPβCyD-IC nanofibrous film was achieved without the use of any organic solvents or toxic agents. The amorphous state of INH and the unique properties of nanofibrous matrix ensured faster and enhanced release profile for INH molecules compared to its pristine powder form. Additionally, INH/HPβCyD-IC nanofibrous film presented a quite fast-disintegration profile in the saliva simulation (~2s). Overall, this approach revealed a promising administration of orally fast-dissolving drug delivery system, especially for pediatric patients.

1. Introduction

Current antibiotic treatments are often administered through oral tablet or intramuscular injections, posing as an obstacle for vulnerable patients, particularly pediatric patients, who often face swallowing challenges and are noncompliant due to the bitter taste [1–3]. The invasiveness of injections and large tablet sizes can deter pediatric patients from complying with treatment, leading to unnecessary deaths from diseases, especially in developing countries [2]. As such, an orally fast dissolving drug delivery system -such as oral strips- for antibiotic drugs is pertinent, as it increases patient compliance, eliminates the need for swallowing, and enhances the bioavailability of the drug at the desired site due to reduced hepatic first pass effect [1,4,5]. Oral strips are free-standing, thin and flexible structures and their hygroscopic nature allows efficient dissolving of these strips on any moist surface, eliminating the need for water [1,4,5]. Furthermore, due to their rapid disintegration in the oral mucosa, the hazard of choking can be significantly reduced. Oral strips are commonly formulized using natural hydrophilic polymers such as pullulan, gelatin, or polyvinyl alcohol (PVA) [6]. On the other hand, cyclodextrins especially their derivates can be a promising alternative for the formulization of orally dissolving strips due to their high-water solubility and ability to form inclusion complexes with a variety of insoluble drugs [7–9]. Cyclodextrins (CyDs) are starch-derived, cyclic oligosaccharides with a hydrophilic exterior and a hydrophobic inner cavity. The donut shape of CyD enables the interaction of a hydrophobic guest molecule with the inner cavity of CyD by forming inclusion complexes and this can allow for enhanced solubility and bioavailability of a poorly water-soluble drugs [7–10]. Moreover, CyD can eliminate the unpleasant taste of drug molecules by inclusion complex formation [11,12].

Orally dissolving strips can be generated using numerous methods such as lyophilization, solvent casting, spraying, extrusion etc. [1,13,

* Corresponding author.
** Corresponding author.
E-mail addresses: ac2873@cornell.edu (A. Celebioglu), tu46@cornell.edu (T. Uyar).
[1] Contributed equally.

https://doi.org/10.1016/j.jddst.2023.104584
Received 19 January 2023; Received in revised form 5 May 2023; Accepted 18 May 2023
Available online 20 May 2023

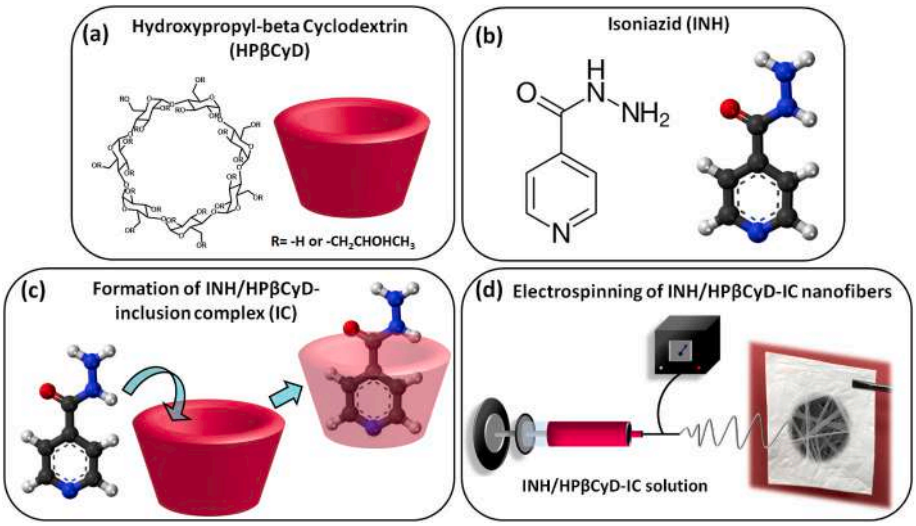

Fig. 1. The concept of study. Chemical structure of (a) hydroxypropyl-beta cyclodextrin (HPβCyD) and (b) isoniazid (INH). Schematic representation of inclusion complex formation between INH and HPβCyD molecules, and electrospinning of INH/HPβCyD-IC nanofibers.

14]. Nanotechnological techniques have also kickstarted development of fast dissolving drug delivery systems. The electrohydrodynamic approach of electrospinning is one of these methods that enables production of free-standing fibrous films which can be loaded with drug molecules [7,15–18]. The high surface area and 3D porous structure of electrospun nanofibers along with drug delivery property makes these functional nanofibrous films an attractive candidate for developing orally fast-dissolving delivery systems [7]. For this purpose, the hydrophilic polymers including poly (ethylene oxide) (PEO) [19], polyvinylpyrrolidone (PVP) [19,20], PVA [19,21], pullulan [22], gelatin [23] and Eudragit [24] have been applied for the generation of nanofibrous fast-dissolving delivery systems. On the other hand, CyD inclusion complexes can be rendered into nanofibrous films without using polymeric carriers or organic toxic solvents through electrospinning technique for creating a fast-dissolving delivery system [25–31].

Isoniazid (isonicotinic acid hydrazide (INH)) is an antimycobacterial drug listed as an essential medicine by the World Health Organization [32]. More recently, INH is gaining recognition not only as an antitubercular drug, but also as a chemotherapeutic drug [33]. However, despite its versatility, INH presents a severely limited bioavailability (~58%) and short half-life (1–4 h), decreasing the permeability of the drug and causing patients to receive multiple doses in high concentrations [33]. Furthermore, INH is currently available only in oral tablet or intramuscular injection form, contributing to patient noncompliance. In particular, due to swallowing and choking hazards for pediatric patients, providers prefer to crush tablets or mix them with food to help with ingestion. However, administration of INH with food can significantly reduce absorption due to its potential to convert into a hydrazone species [32,34]. In a related study, it was found that the INH permeability could only be improved if the dosage was split into three segments, but was otherwise poorly soluble in the stomach, calling for an optimized, noninvasive, fast-dissolving delivery system [35]. In another study, it was theoretically and experimentally proved that, the highly water soluble CyD derivative of hydroxypropyl-beta cyclodextrin (HPβCyD) can enhance the physicochemical properties of INH for the potential treatment of tuberculosis [36]. In this study, HPβCyD was employed for the inclusion complex formation and electrospinning of INH without using an additional polymer or organic solvent for the generation of fast dissolving INH delivery system (Fig. 1). The morphological, structural, and pharmaco-technical properties of these electrospun nanofibrous films were analyzed through proper techniques and approaches.

2. Materials and methods

2.1. Materials

Isoniazid (Isonicotinic acid hydrazide (INH), (98%, TCI), for buffer solutions; phosphate buffered saline tablet (Sigma Aldrich), sodium phosphate dibasic heptahydrate (Na_2HPO_4, 98.0−102.0%, Fisher Chemical), sodium chloride (NaCl, >99%, Sigma-Aldrich), potassium phosphate monobasic (KH_2PO_4, ≥99.0%, Fisher Chemical), *o*-phosphoric acid (85%, Fisher Chemical), hydrochloric acid (Sigma-Aldrich, Ph. Eur., BP, NF, fuming, 36.5–38%) and deuterated dimethyl sulfoxide (DMSO-d_6, deuteration degree min. 99.8%, Cambridge Isotope) were provided commercially. Hydroxypropyl-beta cyclodextrin (HPβCyD) (Cavasol® W7 HP, standard grade, DS: ~0.9) was kindly gifted from Wacker Chemie AG (USA). The Millipore Milli-Q ultrapure water system was employed for distilled water.

2.2. Preparation of inclusion complex systems

A clear solution of HPβCyD was prepared at a solid concentration of 200% (w/v) in distilled water. Then, INH powder was added to the this HPβCyD solution so as to provide 1/1 M ratio (INH/HPβCyD), such that there was ~8% (w/w) of INH content in proportion to the total sample amount. The INH/HPβCyD solution was stirred for 24 h at room temperature to form inclusion complexes (IC). As a control sample, pure HPβCyD solution was also prepared at a concentration of 200% (w/v). The conductivity and viscosity of HPβCyD and INH/HPβCyD-IC solutions were measured prior the electrospinning. Here, a conductivity-meter was used (FiveEasy, Mettler Toledo, USA) at room temperature to detect the conductivity of systems and viscosity was measured by a rheometer (AR 2000 rheometer, TA Instrument, USA, 20 mm, 4° cone-plate spindle) at a shear rate of 0.01–1000 s^{-1} at 20 °C.

2.3. Electrospinning process

First, 1 ml of plastic syringes clipped with a 27 G needle were separately loaded with the homogenous solutions of HPβCyD and INH/HPβCyD-IC. Then, these syringes were pushed using a syringe pump with the flow rate of 0.5 mL/h. The fixed aluminum collector covered with aluminum foil was located 15 cm away from needle and nanofibers were deposited on this collector by applying a voltage of 17.5 kV. The process was performed in an electrospinning equipment (Spingenix, model: SG100, Palo Alto, USA). The temperature and relative humidity

Table 1
Solution properties and average fiber diameters (AFD) of electrospun nanofibers.

Sample	HPβCyD conc. (%, w/v)	INH conc. (%, w/w)	Viscosity (Pa·s)	Conductivity (μS/cm)	AFD (mean ± std deviation) (nm)
HPβCyD	200	–	1.12	37.66	225 ± 95
INH/HPβCyD-IC	200	8	1.03	30.77	410 ± 215

during the process were noted as 21 °C and 38%, respectively.

2.4. Structural characterizations

The morphology of HPβCyD nanofibers and INH/HPβCyD-IC nanofibers were detected using scanning electron microscopy (SEM, Tescan MIRA3, Czech Republic). Prior to placement in the SEM, samples were coated with thin layer of Au/Pd. To calculate the average fiber diameter (AFD), ImageJ software was used upon calculating ~ 80 fibers for both the HPβCyD and INH/HPβCyD-IC nanofibers.

The loading efficiency of INH/HPβCyD-IC nanofibers was calculated through proton nuclear magnetic resonance spectroscopy (^{1}H NMR). The solutions were prepared by separately dissolving pure INH, HPβCyD nanofibers, and INH/HPβCyD-IC nanofibers in DMSO-d_6. The samples were then placed in the ^{1}H NMR spectrometer (Bruker AV500, with autosampler). The ^{1}H NMR spectra was recorded using 16 scanning. To determine the molar ratio (INH/HPβCyD), and so the loading efficiency of samples, the results were analyzed using Mestrenova software by integrating the non-overlapping peaks of both components.

The presence of an inclusion complex within INH/HPβCyD-IC nanofibers was confirmed using various technique and Fourier transform infrared spectroscopy (FTIR), differential scanning calorimetry (DSC), and thermogravimetric analysis (TGA) is one of them. The FTIR spectra (32 scans) of pure INH, HPβCyD nanofibers and INH/HPβCyD-IC nanofibers were recorded using attenuated total reflectance FTIR (ATR-FTIR) spectrometer (PerkinElmer, USA) in the range of 4000–600 cm^{-1} and at a resolution of 4 cm^{-1}. X-ray diffractometer (Bruker D8 Advance ECO, Germany) was also used to analyze the conversion from crystalline to amorphous state of INH by inclusion complexation within INH/HPβCyD-IC nanofibers (40 kV, 25 mA, $2\Theta = 5°$-$30°$, Cu-Kα radiation). The amorphization of INH was also checked using the thermal characterization approach of differential scanning calorimeter (DSC) (TA Instruments Q2000, USA). To obtain DSC thermograms, pure INH, HPβCyD, and INH/HPβCyD-IC nanofibers were placed in a T-zero aluminum pan separately and heated from 0 °C to 200 °C in increments of 10 °C/min. Additionally, thermal degradation of samples was examined using thermal gravimetric analyzer (TGA) (TA Instruments Q500, USA). Each sample was placed on the platinum pan and heated from room temperature to 600 °C at a rate of 20 °C/min in thermogravimeter.

2.5. Pharmacotechnical properties

The time dependent *in-vitro* release tests were performed for pure INH and INH/HPβCyD-IC nanofibers in three different buffer solutions having pH 7.4, pH 6.8 and pH 1.2 values. For this, ~20 mg of INH/HPβCyD-IC nanofibrous film was immersed in 10 mL of buffer solutions and shaken on the orbital shaker at 200 rpm at 37 °C. The amount of INH powder (~1.7 mg) was arranged to provide the same drug content of

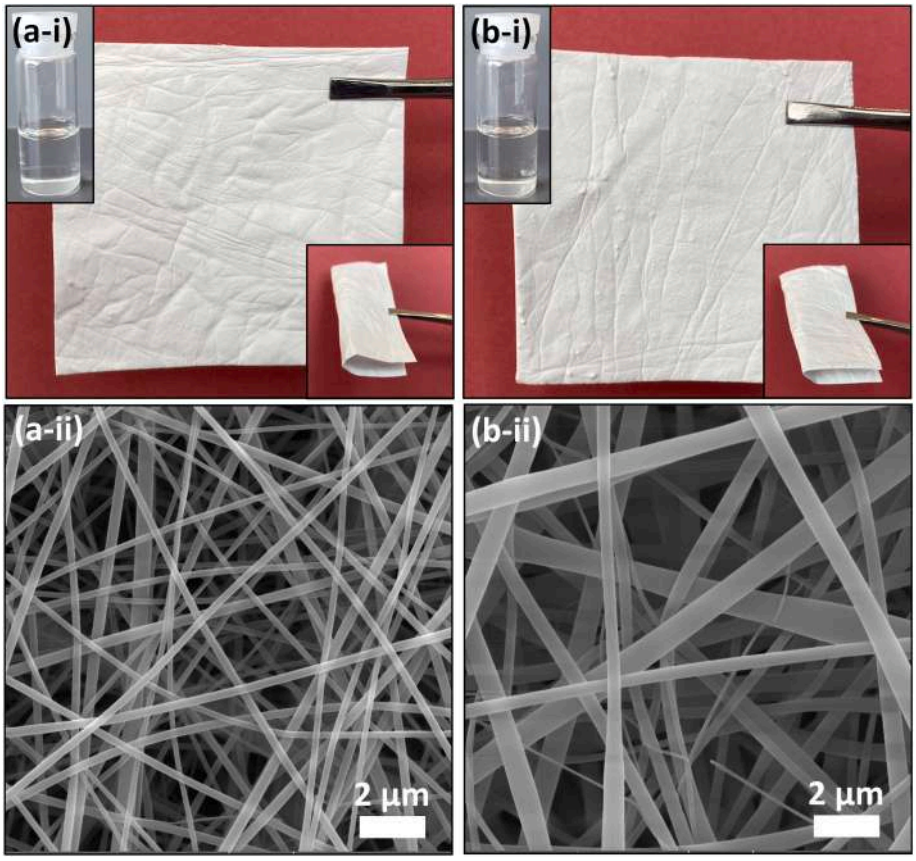

Fig. 2. The visual and morphological analysis. Photographs of (i) electrospinning solutions and resulting electrospun nanofibers, and (ii) respective SEM images of (a) HPβCyD nanofibers and (b) INH/HPβCyD-IC nanofibers.

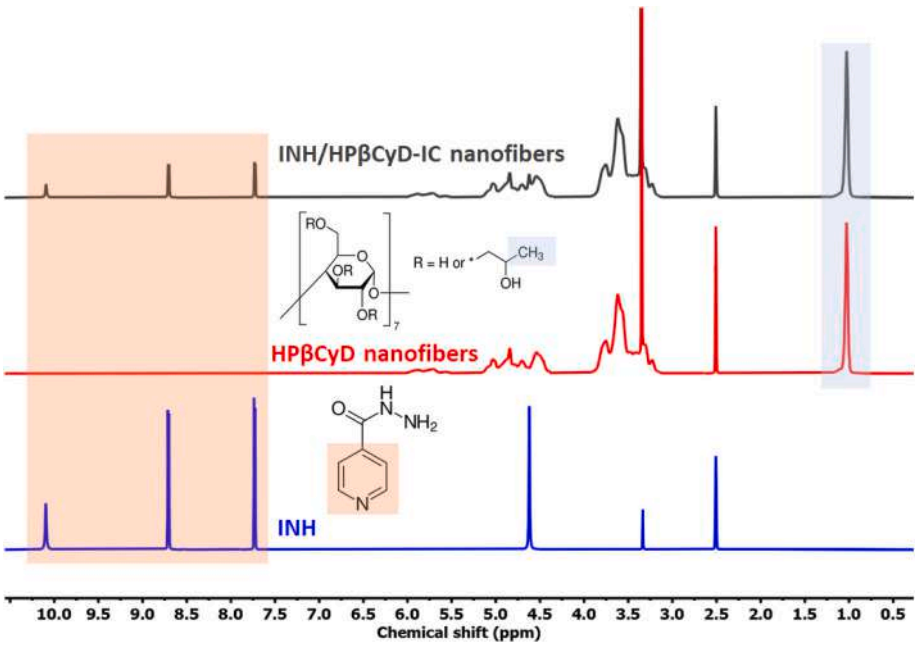

Fig. 3. The chemical characterization. ^{1}H NMR spectra of INH/HPβCyD-IC nanofibers, HPβCyD nanofibers, and INH.

used nanofibrous film (~20 mg) for the release test. Aliquots of 500 μL were removed from release environment and replaced with 500 μL of fresh buffer at specific time intervals. The aliquots were then measured by UV–vis spectroscopy (PerkinElmer, Lambda 35, USA) (263 nm) to calculate the release percentage of the drug. The calculation was performed through a calibration curve ($R^2 \geq 0.99$) and mean ± standard deviation of all trials plotted with respect to time using the results of at least three measurements for each sample and buffer systems.

Through the disintegration test, the behavior of HPβCyD nanofibers and INH/HPβCyD-IC nanofibers were examined in a medium that emulated the oral cavity moist environment. Here, a filter paper was placed in a plastic Petri dish (10 cm) and then wetted with 5 mL of artificial saliva (pH = 6.8; 2.38 g Na_2HPO_4, 0.190 g KH_2PO_4, 8 g NaCl and few drops of phosphoric acid in 1 L water). Afterwards, the excess artificial saliva was removed from the Petri dish. Nanofibrous film of HPβCyD and INH/HPβCyD-IC having the approximate size of 6 cm × 7 cm was placed on the filter paper wetted with the artificial saliva and the disintegration behavior was concurrently recorded as a video (Video S1).

2.6. Statistical analyses

The statistical analyses for characterizations were performed through Origin Lab (Origin, 2022, USA) and an online calculator. For all replicated experiments, the values were given as value ± standard deviation. The ANOVA analysis was used to measure significance at a 0.05 level of probability.

3. Results and discussion

3.1. Morphology of nanofibers

The INH/HPβCyD-IC nanofiber was prepared using 200% (w/v) of CyD concentration and at a 1/1 M ratio (drug/CyD), where INH composed ~ 8% (w/w) content of the nanofiber. Meanwhile, the control sample of pure HPβCyD nanofibers was prepared at the same CyD concentration of 200% (w/v) (Table 1). Due to CyD's ability to form aggregates through hydrogen bonds, a high concentration of CyD was necessary in order to aid in fiber formation during electrospinning [25]. Fig. 2 presents the photos of electrospinning solutions and nanofibrous films, and SEM images of the HPβCyD and INH/HPβCyD-IC nanofibers. Here, both HPβCyD and INH/HPβCyD-IC systems yielded clear homogenous solutions (Fig. 2a, b-i). Considering the clear solution of the INH/HPβCyD-IC system, it is evident that INH powder was able to fully dissolve due to complex formation with HPβCyD at 1/1 M ratio. As a result of electrospinning, INH/HPβCyD-IC nanofibers presented flexible, and freestanding structure, similar to the pure HPβCyD nanofiber (Fig. 2a,b-i). SEM imaging revealed the defect-free and homogenous fiber morphology for both nanofibrous films (Fig. 2a,b-ii). Table 1 summarizes the average fiber diameter (AFD) (mean ± std deviation) of nanofibers, and conductivity/viscosity values of their electrospinning solutions. Visibly confirmed by the SEM images, the AFD of the INH/HPβCyD-IC nanofibers are higher (410 ± 215 nm) than that of pure HPβCyD nanofibers (225 ± 95 nm). Through the statistical analyses, it was found that the average diameters are significantly different from each other ($p < 0.05$). The conductivity of INH/HPβCyD-IC solution (30.77 μS/cm) is lower than pure HPβCyD solution (37.66 μS/cm). On the other hand, the viscosity of INH/HPβCyD-IC solution (1.03 Pa s) is slightly different from HPβCyD one (1.12 Pa s). Here, the lower conductivity of INH/HPβCyD-IC system can be the explanation of thicker fiber formation than HPβCyD system since it was exposed less stretching during electrospinning process due to less amount of electrical charge in the electrospinning solution [37].

3.2. Structural characterizations

The aqueous solution of INH/HPβCyD-IC was originally prepared using a 1/1 (drug/CyD) molar ratio which corresponds to the ~8% (w/w) of INH content in the nanofiber. Through ^{1}H NMR analysis, the loading efficiency was determined and Fig. 3 depicts the ^{1}H NMR spectra of pure INH, HPβCyD nanofibers, and the INH/HPβCyD-IC nanofibers. The highlighted regions represent the non-overlapping peaks of INH and HPβCyD that were integrated to calculate the molar ratio. Specifically, the characteristic peak of HPβCyD located at 1.03 ppm (-CH_3) was integrated due to its distinct presence both in HPβCyD and INH/HPβCyD-IC nanofibers [25]. Here, INH was integrated using the characteristic peaks locating in the range of 7.5–10.5 ppm which represent the aromatic ring of drug molecule (Fig. 3) [36,38]. Through this method, a ratio of ~1/1 (INH/HPβCyD) was found, indicating complete preservation of the original ratio, and suggesting a ~100% of loading

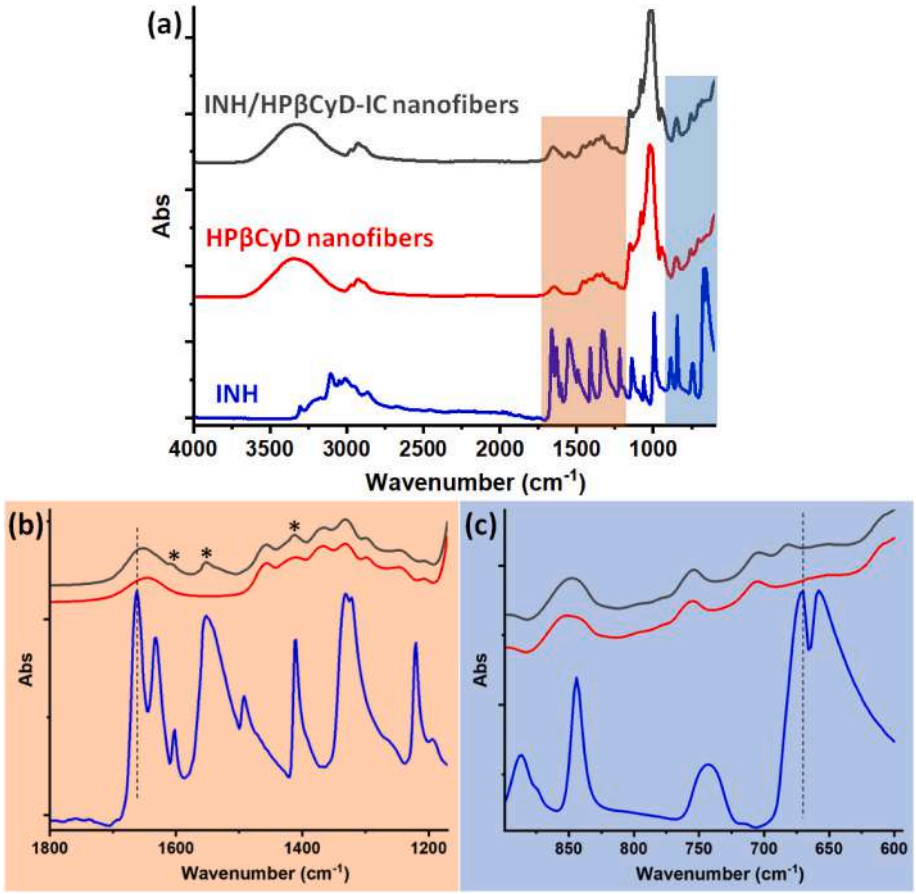

Fig. 4. The chemical characterization. FTIR spectra of pure INH, HPβCyD nanofibers, and INH/HPβCyD-IC nanofibers; (a) full range, (b) & (c) expanded range of notable regions.

efficiency and ~8% (w/w) of INH content of final nanofibers. Considering the characteristic peaks of INH, they were observed with the same pattern in the case of INH/HPβCyD-IC nanofibers. This can also be concluded that the chemical structure of INH was preserved during all preparation and electrospinning processes. As such, in line with previous studies, INH and HPβCyD can efficiently form inclusion complexes with a 1/1 M ratio (INH/HPβCyD) [36,38].

Fig. 4 presents the FTIR spectra of pure INH, HPβCyD nanofibers, and the INH/HPβCyD-IC nanofibers. The disappearances and/or shifts of certain characteristic peaks observed in the FTIR spectrum can provide insights on the bonding between host and guest molecules by inclusion complexation [39,40]. Referring to HPβCyD nanofibers, a characteristic peak occurs at 3400 cm^{-1}, representing the stretching of –OH groups of the primary/secondary hydroxyl groups of HPβCyD [39,41]. The absorption peaks at 1028 cm^{-1}, 1150 cm^{-1}, 1180 cm^{-1}, 1370 cm^{-1}, 1650 cm^{-1} and 2930 cm^{-1} correspond to coupled *C*–C/C–O stretching, antisymmetric *C*–*O*–C glycosidic bridge stretching, –CH_3 bending, O–H bending and *C*–H stretching of CyD, respectively (Fig. 4a) [39,41]. The unique characteristic peaks of pure HPβCyD nanofiber are most likely also observed in the INH/HPβCyD-IC nanofibers due to the immensely high portion of HPβCyD in the sample structure (~92% (w/w)) [25]. For INH molecule, there were absorption peaks at 1662 cm^{-1}, 1633 cm^{-1}, 1552 cm^{-1} and 1411 cm^{-1} which are respectively corresponding to C═O, asymmetric *C*–N, NH/C═N and C═C stretching (Fig. 4b) [42]. All the peaks of INH highlighted in the given expanded FTIR region (Fig. 4b) were also observed in the FTIR graph of INH/HPβCyD-IC nanofibers and this proved the existence of drug molecules in the electrospun nanofibers. For characteristic peak of INH at 1662 cm^{-1}, there was detected a shift in case of INH/HPβCyD-IC nanofibers to the 1654 cm^{-1} confirming the presence of the inclusion complexation. In the second expanded FTIR region (Fig. 4b), a strong absorption peak at 657 cm^{-1} of INH corresponds to *C*–C–C bending and the shift to 677 cm^{-1} in case of INH/HPβCyD-IC nanofibers are also another indication for the inclusion complex formation between INH and HPβCyD.

XRD was employed to analyze potential changes in crystal structure of INH which can be occurred by inclusion complexation with HPβCyD. Fig. 5a presents the XRD patterns of pure INH, HPβCyD nanofibers, and INH/HPβCyD-IC nanofibers. Pure INH exhibits a crystalline structure; as such, characteristic diffraction peaks can be observed at 12.2°, 14.5°, 17.9°, 25.3°, 27.5°. For HPβCyD nanofibers, broad halos are observed at ~10° and 18.5° due its amorphous nature. The crystalline peaks observed for INH are not observed in the INH/HPβCyD-IC nanofibers; rather, broad halos similar to the ones observed in pure HPβCyD nanofibers were exhibited, indicating that INH follows an amorphous distribution within nanofibers due to inclusion complexation. The amorphization of INH can be further confirmed through DSC characterization. Fig. 5b depicts the DSC thermograms of pure INH, HPβCyD nanofibers, and INH/HPβCyD-IC nanofibers. Pure INH expressed a distinct endothermic peak at ~171 °C corresponding its melting point. On the other hand, both HPβCyD and INH/HPβCyD-IC nanofibers displayed a broad endothermic peak at ~90 °C, corresponding to the dehydration of water. Here, the crystalline melting point of pure INH was absent in the INH/HPβCyD-IC nanofibers. As such, it can be further concluded that INH transitioned into an amorphous state within the inclusion complex, aligning with the results observed for XRD analysis.

Thermal degradation profile of samples was analyzed through TGA technique. Fig. 6 shows the TGA thermograms and their derivate graphs (DTG) for INH, HPβCyD nanofibers, and INH/HPβCyD-IC nanofibers. For HPβCyD nanofibers, a two-step weight loss is present where the first weight loss occurs till ~100 °C due to water dehydration and the second

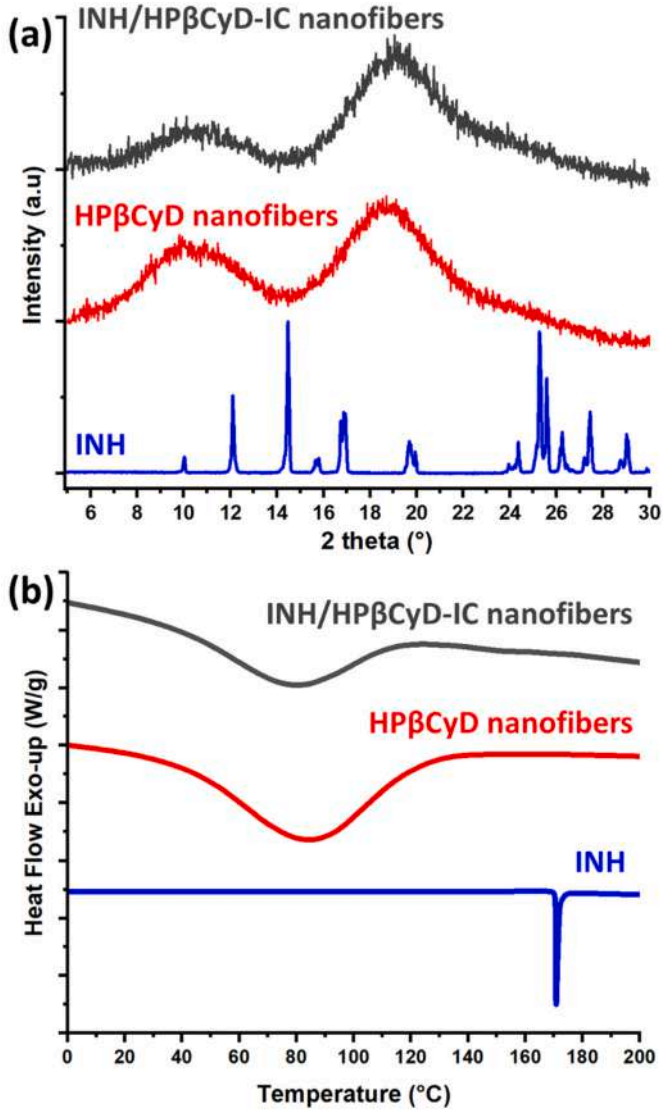

Fig. 5. The crystallinity analysis. (a) XRD graphs and (b) DSC thermograms of INH, HPβCyD nanofibers, and INH/HPβCyD-IC nanofibers.

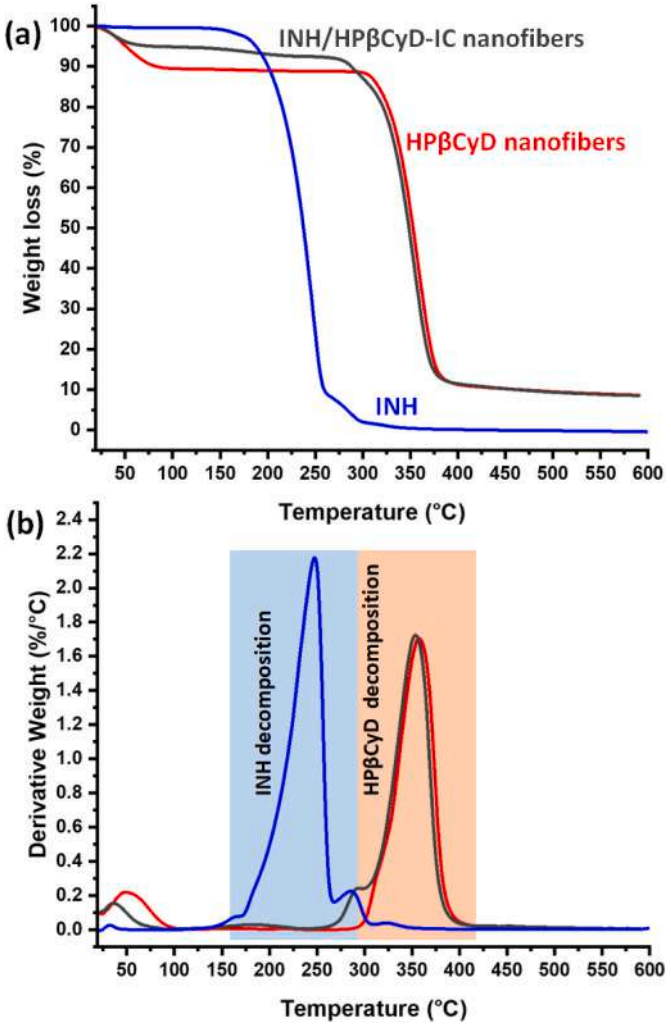

Fig. 6. Thermal characterization. (a) TGA thermograms and (b) derivates (DTG) of INH, HPβCyD nanofibers, and INH/HPβCyD-IC nanofibers.

significant weight loss occurs at ~350 °C due to the degradation of HPβCyD. A two-step degradation profile having similar weight losses can be also observed for INH/HPβCyD-IC nanofibers. However, there is also a shoulder at ~294 °C differently from HPβCyD nanofibers as it is obvious from DTG. On the other hand, the TGA thermogram for pure INH showed a main degradation point occur at ~247 °C. There was also detected a small weight loss at ~286 °C for INH. It is clear from DTG of INH/HPβCyD-IC nanofibers that the shoulder at 294 °C originated from the INH content in the samples. Since it was covered by the main degradation step of HPβCyD and the HPβCyD content (~92% (w/w)) is significantly higher than the INH (~8% (w/w)), it was not possible to examine INH content from TGA findings. However, the shifts to the higher temperature range in thermal degradation of INH in case of INH/HPβCyD-IC nanofibers signified the interactions between INH and HPβCyD molecules by inclusion complex formation.

3.3. Pharmacotechnical profiles

Time dependent *in-vitro* release test was performed for INH/HPβCyD-IC nanofibers and pure INH in three different pH values; 7.4, 6.8 and 1.2 representing physiological, intestinal and stomach environment, respectively. Fig. 7 shows the release profiles of these two samples in given pH values. Here, INH reached the maximum release values of ~52%, ~55%, and ~57% in pH 7.4, pH 6.8, and pH 1.2, respectively in different time points (2, 8 and 4 min) over 10 min release period (Fig. 7).

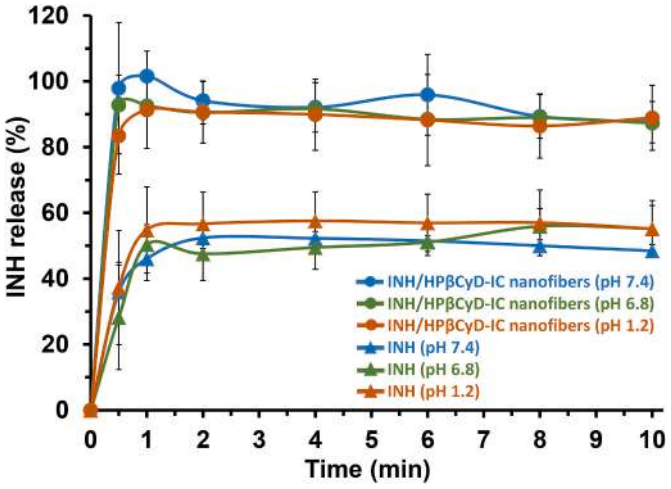

Fig. 7. Time dependent release test. Release profiles of INH and INH/HPβCyD-IC nanofibers.

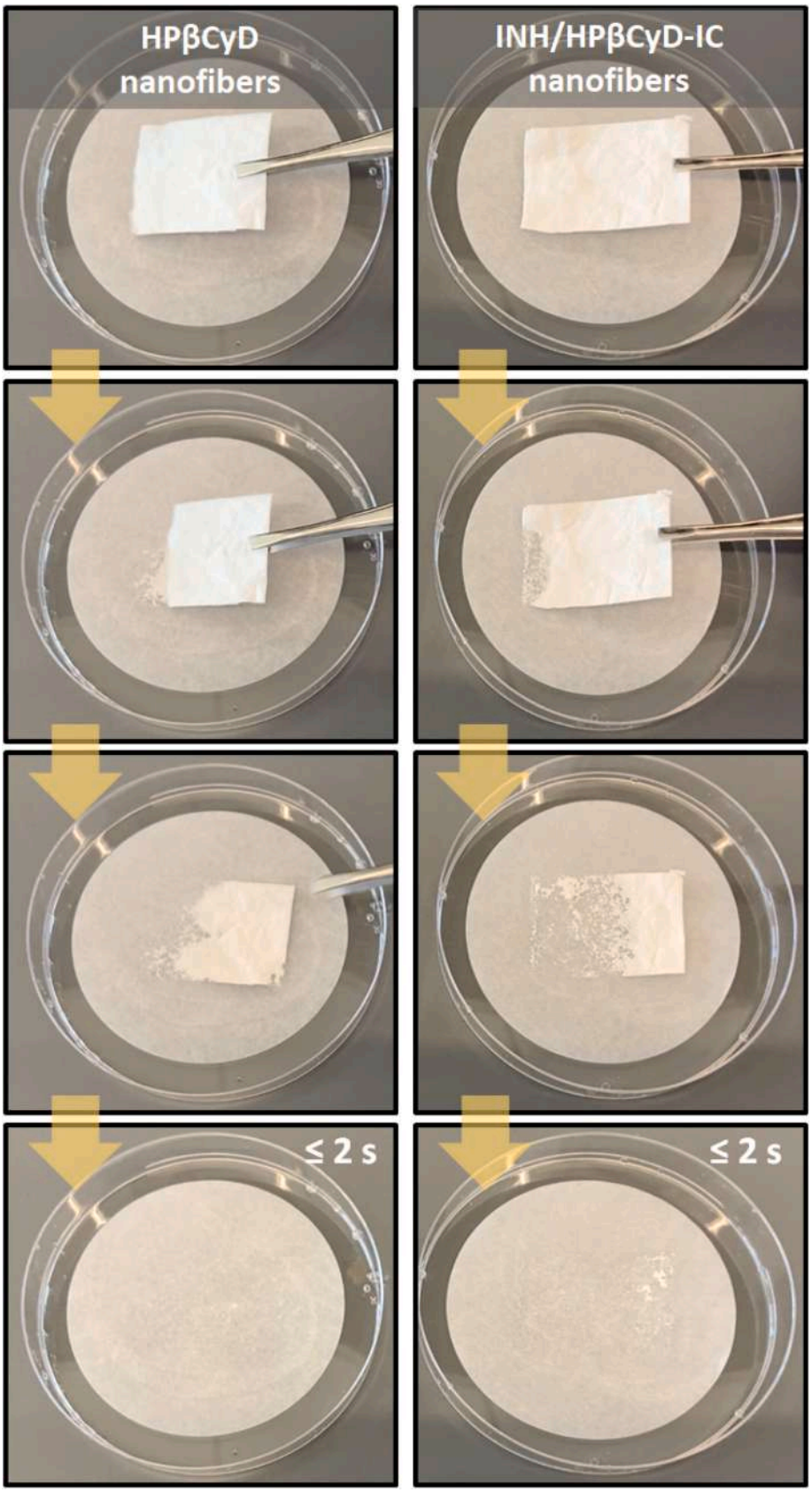

Fig. 8. The artificial saliva test. Disintegration profile of HPβCyD nanofibers and INH/HPβCyD-IC nanofibers.

On the other hand, the release of INH/HPβCyD-IC nanofibers were respectively ~100%, ~92%, and ~91% in pH 7.4, pH 6.8, and pH 1.2 environments in 1 min most the latest. Statistical analyses of the release between the INH/HPβCyD-IC nanofibers and INH showed to be significantly different ($p < 0.05$) from each other, however not significantly different for different pH values ($p > 0.05$). As such, the findings conveyed that the inclusion complexation of INH with HPβCyD significantly enhanced the release profile compared to pure INH in its pure crystalline form. This is likely due to the amorphous distribution of drug which provided an improved solubility for INH molecule. It is also apparent that INH/HPβCyD-IC nanofibers can ensure an enhanced release profile for different pH values suggesting the efficient absorption of this drug in all given environments. Kinetic models were also applied to further analyze the release behavior of samples. Table S1 summarized the R^2 (regression coefficient) values obtained using different kinetic model calculation. The results showed that both INH and INH/HPβCyD-IC nanofibers did not exhibit compatibility with neither zero/first-order kinetics nor Higuchi models (Table S1). This revealed that Fick's first law which displays the time-dependent release of drugs from insoluble substrate, did not rule the release profile of samples [43]. On the other hand, Korsmeyer-Peppas model exhibited relatively better consistency compared to other models for both INH and INH/HPβCyD-IC nanofibers (Table S1) and this supported the diffusion and erosion-dependent release of INH. The diffusion exponent (n) values determined by Korsmeyer–Peppas equations were found in the range of $0.45 < n < 0.89$ confirming the irregular diffusion and non-Fickian release of drug molecules in the liquid medium [43].

To understand the behavior of the INH/HPβCyD-IC nanofibers within oral mucosa, the disintegration test was conducted using an artificial saliva. The disintegration profile of INH/HPβCyD-IC nanofibers was compared with the control of pure HPβCyD nanofibers. Fig. 8 presents the disintegration profile of HPβCyD and INH/HPβCyD-IC nanofibers captured from Video S1. As seen from the profile, both nanofibers completely disintegrated within 2 s of contact with the artificial saliva (Fig. 8). For both fast-release and fast-disintegration profile, it can be concluded that the high-water solubility of HPβCyD (>2000 mg/mL), the high porosity and high surface area to volume ratio of nanofibrous films contributed to penetration of water through the samples to ensure high number of active contact side for liquid medium. All these make INH/HPβCyD-IC nanofibers an exceptional candidate as an orally fast-dissolving delivery system.

4. Conclusions

In this study, the polymer-free nanofibrous film of INH/HPβCyD-IC was generated with uniform morphology having ~400 nm of average fiber diameter. INH/HPβCyD-IC nanofibers were obtained without using a toxic solvent or chemical in water. The amorphous distribution of INH within the nanofibrous film of INH/HPβCyD-IC was provided by inclusion complexation in HPβCyD cavity. The INH/HPβCyD-IC system was initially prepared to have a 1/1 M ratio corresponding to INH loading of ~8% (w/w) and it was protected throughout the process, thus the ultimate INH/HPβCyD-IC nanofibers were obtained with ~100% loading efficiency. Here, the unique properties of electrospun nanofibers including high surface area and high porosity, and the high solubility of HPβCyD (>2000 mg/mL) matrix promoted the fast dissolution of INH/HPβCyD-IC nanofibers in the aqueous medium. Besides these factors, the amorphous distribution of INH in INH/HPβCyD-IC nanofibers provided a faster release of the drug compared to its pristine powder form. Additionally, INH/HPβCyD-IC nanofibers showed a fast-disintegration property in the artificial saliva (~2 s). The nanofibrous film of inclusion complexes can be applied for the treatment of antibiotic drug molecules of INH. The orally fast-dissolving INH/HPβCyD-IC nanofibers can be an accomplished option against the commercial formulations of INH. As such, with the elimination of tablet or injection administration and the unflattering taste of INH, increased pediatric patient compliance might be possible by making INH/HPβCyD-IC nanofibers to current treatment options. Moreover, further investigations to form electrospun nanofibrous films of alternate essential antibiotics using HPβCyD inclusion complexes would be highly beneficial to the understanding of future fast-dissolving drug delivery systems.

CRediT authorship contribution statement

Spoorthi Patil: Investigation, Writing – original draft. **Asli Celebioglu:** Conceptualization, Methodology, Investigation, Writing – original draft. **Tamer Uyar:** Conceptualization, Methodology, Writing – review & editingEditing, Funding acquisition, Project administration.

Declaration of competing interest

The authors declare that they have no known competing financial interests or personal relationships that could have appeared to influence the work reported in this paper.

Data availability

Data will be made available on request.

Acknowledgement

The work was made possible by the Cornell Center for Materials Research Shared Facilities which are supported through the NSF MRSEC program (DMR-1719875), and the Cornell Chemistry NMR Facility supported in part by the NSF MRI program (CHE-1531632), and Department of Human Centered Design facilities. S.P. acknowledges the work was also made possible by the Cornell University Engineering Learning Initiatives (ELI) Summer Grant (Wood Excellence Edu).

Appendix A. Supplementary data

Supplementary data related to this article can be found at https://doi.org/10.1016/j.jddst.2023.104584.

References

[1] R. Bala, S. Khanna, P. Pawar, S. Arora, Orally dissolving strips: a new approach to oral drug delivery system, Int. J. Pharm. Investig. 3 (2013) 67–76.
[2] J. Boateng, Drug delivery innovations to address global health challenges for pediatric and geriatric populations (through improvements in patient compliance), J. Pharmaceut. Sci. 106 (2017) 3188–3198.
[3] E.A. Kean, O.A. Adeleke, Orally disintegrating drug carriers for paediatric pharmacotherapy, Eur. J. Pharmaceut. Sci. 182 (2023), 106377.
[4] M. He, L. Zhu, N. Yang, H. Li, Q. Yang, Recent advances of oral film as platform for drug delivery, Int. J. Pharm. 604 (2021), 120759.
[5] E. Turković, I. Vasiljević, M. Drašković, J. Parojčić, Orodispersible films—pharmaceutical development for improved performance: a review, J. Drug Deliv. Sci. Technol. (2022), 103708.
[6] D. Sharma, D. Kaur, S. Verma, D. Singh, M. Singh, G. Singh, R. Garg, Fast dissolving oral films technology: a recent trend for an innovative oral drug delivery system, Int. J. Drug Deliv. 7 (2015) 60–75.
[7] B. Balusamy, A. Celebioglu, A. Senthamizhan, T. Uyar, Progress in the design and development of "fast-dissolving" electrospun nanofibers based drug delivery systems - a systematic review, J. Contr. Release 326 (2020) 482–509.
[8] G. Crini, A history of cyclodextrins, Chem. Rev. 114 (2014) 10940–10975.
[9] P. Jansook, N. Ogawa, T. Loftsson, Cyclodextrins: structure, physicochemical properties and pharmaceutical applications, Int. J. Pharm. 535 (2018) 272–284.
[10] S.S. Braga, Cyclodextrin superstructures for drug delivery, J. Drug Deliv. Sci. Technol. (2022), 103650.
[11] W. Samprasit, P. Akkaramongkolporn, R. Kaomongkolgit, P. Opanasopit, Cyclodextrin-based oral dissolving films formulation of taste-masked meloxicam, Pharmaceut. Dev. Technol. 23 (2018) 530–539.
[12] S. Mohapatra, A. Bose, S. Bindhani, R.K. Kar, N.R. Pani, A.K. Nayak, Effect of hydrophilic polymer on solubility and taste masking of linezolid in multi-component cyclodextrin inclusion complex: physicochemical characterization and molecular docking, J. Drug Deliv. Sci. Technol. 66 (2021), 102876.
[13] V.F. Patel, F. Liu, M.B. Brown, Advances in oral transmucosal drug delivery, J. Contr. Release 153 (2011) 106–116.
[14] R.D. Rahane, P.R. Rachh, A review on fast dissolving tablet, J. Drug Deliv. Therapeut. 8 (2018) 50–55.

[15] D.-G. Yu, J.-J. Li, G.R. Williams, M. Zhao, Electrospun amorphous solid dispersions of poorly water-soluble drugs: a review, J. Contr. Release 292 (2018) 91–110.
[16] A. Celebioglu, A.F. Saporito, T. Uyar, Green electrospinning of chitosan/pectin nanofibrous films by the incorporation of cyclodextrin/curcumin inclusion complexes: pH-responsive release and hydrogel features, ACS Sustain. Chem. Eng. 10 (2022) 4758–4769.
[17] Y. Si, S. Shi, J. Hu, Applications of electrospinning in human health: from detection, protection, regulation to reconstruction, Nano Today 48 (2023), 101723.
[18] S.M. Tan, X.Y. Teoh, J. Le Hwang, Z.P. Khong, R. Sejare, A.Q.A. Al Mashhadani, R. Abou Assi, S.Y. Chan, Electrospinning and its potential in fabricating pharmaceutical dosage form, J. Drug Deliv. Sci. Technol. (2022), 103761.
[19] N. Sharifi, S.A. Mortazavi, S. Rabbani, M. Torshabi, R. Talimi, A. Haeri, Fast dissolving nanofibrous mats for diclofenac sodium delivery: effects of electrospinning polymer and addition of super-disintegrant, J. Drug Deliv. Sci. Technol. (2022), 103356.
[20] H. Bukhary, G.R. Williams, M. Orlu, Electrospun fixed dose formulations of amlodipine besylate and valsartan, Int. J. Pharm. 549 (2018) 446–455.
[21] S. Nam, S.Y. Lee, H.-J. Cho, Phloretin-loaded fast dissolving nanofibers for the locoregional therapy of oral squamous cell carcinoma, J. Colloid Interface Sci. 508 (2017) 112–120.
[22] E. Hsiung, A. Celebioglu, R. Chowdhury, M.E. Kilic, E. Durgun, C. Altier, T. Uyar, Antibacterial nanofibers of pullulan/tetracycline-cyclodextrin inclusion complexes for Fast-Disintegrating oral drug delivery, J. Colloid Interface Sci. 610 (2022) 321–333.
[23] Z. Aytac, S. Ipek, I. Erol, E. Durgun, T. Uyar, Fast-dissolving electrospun gelatin nanofibers encapsulating ciprofloxacin/cyclodextrin inclusion complex, Colloids Surf. B Biointerfaces 178 (2019) 129–136.
[24] P.S. Giram, A. Shitole, S.S. Nande, N. Sharma, B. Garnaik, Fast dissolving moxifloxacin hydrochloride antibiotic drug from electrospun Eudragit L-100 nonwoven nanofibrous Mats, Mater. Sci. Eng., C 92 (2018) 526–539.
[25] E. Hsiung, A. Celebioglu, M.E. Kilic, E. Durgun, T. Uyar, Ondansetron/Cyclodextrin inclusion complex nanofibrous webs for potential orally fast-disintegrating antiemetic drug delivery, Int. J. Pharm. 623 (2022), 121921.
[26] A. Celebioglu, N. Wang, M.E. Kilic, E. Durgun, T. Uyar, Orally fast disintegrating cyclodextrin/prednisolone inclusion-complex nanofibrous webs for potential steroid medications, Mol. Pharm. 18 (2021) 4486–4500.
[27] A. Celebioglu, T. Uyar, Electrospun formulation of acyclovir/cyclodextrin nanofibers for fast-dissolving antiviral drug delivery, Mater. Sci. Eng., C 118 (2021), 111514.
[28] A. Celebioglu, T. Uyar, Metronidazole/Hydroxypropyl-β-Cyclodextrin inclusion complex nanofibrous webs as fast-dissolving oral drug delivery system, Int. J. Pharm. 572 (2019), 118828.
[29] S. Gao, W. Feng, H. Sun, L. Zong, X. Li, L. Zhao, F. Ye, Y. Fu, Fabrication and characterization of antifungal hydroxypropyl-β-cyclodextrin/pyrimethanil inclusion compound nanofibers based on electrospinning, J. Agric. Food Chem. 70 (2022) 7911–7920.
[30] S. Gao, J. Jiang, X. Li, F. Ye, Y. Fu, L. Zhao, Electrospun polymer-free nanofibers incorporating hydroxypropyl-β-cyclodextrin/difenoconazole via supramolecular assembly for antifungal activity, J. Agric. Food Chem. 69 (2021) 5871–5881.
[31] S. Gao, X. Li, G. Yang, W. Feng, L. Zong, L. Zhao, F. Ye, Y. Fu, Antibacterial perillaldehyde/hydroxypropyl-γ-cyclodextrin inclusion complex electrospun polymer-free nanofiber: improved water solubility, thermostability, and antioxidant activity, Ind. Crop. Prod. 176 (2022), 114300.
[32] D.J. Klein, S. Boukouvala, E.M. McDonagh, S.R. Shuldiner, N. Laurieri, C.F. Thorn, R.B. Altman, T.E. Klein, PharmGKB summary: isoniazid pathway, pharmacokinetics (PK), Pharmacogenetics Genom. 26 (2016) 436–444.
[33] D.R. Telange, R.R. Pandharinath, A.M. Pethe, S.P. Jain, P.L. Pingale, Calcium ion-sodium alginate-piperine-based microspheres: evidence of enhanced encapsulation efficiency, bio-adhesion, controlled delivery, and oral bioavailability of isoniazid, AAPS PharmSciTech 23 (2022) 1–18.
[34] R. Bhandari, I.P. Kaur, Pharmacokinetics, tissue distribution and relative bioavailability of isoniazid-solid lipid nanoparticles, Int. J. Pharm. 441 (2013) 202–212.
[35] T.T. Mariappan, S. Singh, Regional gastrointestinal permeability of rifampicin and isoniazid (alone and their combination) in the rat, Int. J. Tubercul. Lung Dis. 7 (2003) 797–803.
[36] M.G. Teixeira, J. V de Assis, C.G.P. Soares, M.F. Venancio, J.F. Lopes, C. S. Nascimento Jr., C.P.A. Anconi, G.S.L. Carvalho, C.S. Lourenco, M. V de Almeida, Theoretical and experimental study of inclusion complexes formed by isoniazid and modified β-cyclodextrins: 1H NMR structural determination and antibacterial activity evaluation, J. Phys. Chem. B 118 (2014) 81–93.
[37] J. Xue, T. Wu, Y. Dai, Y. Xia, Electrospinning and electrospun nanofibers: methods, materials, and applications, Chem. Rev. 119 (2019) 5298–5415.
[38] J. V de Assis, M.G. Teixeira, C.G.P. Soares, J.F. Lopes, G.S.L. Carvalho, M.C. S. Lourenço, M. V De Almeida, W.B. de Almeida, S.A. Fernandes, Experimental and theoretical NMR determination of isoniazid and sodium p-sulfonatocalix [n] arenes inclusion complexes, Eur. J. Pharmaceut. Sci. 47 (2012) 539–548.
[39] G. Narayanan, R. Boy, B.S. Gupta, A.E. Tonelli, Analytical techniques for characterizing cyclodextrins and their inclusion complexes with large and small molecular weight guest molecules, Polym. Test. 62 (2017) 402–439.
[40] M. Pradhan, B. Nanda, S.R. Panda, P. Kar, B.B. Nanda, Exploration of intermolecular interactions of the anti-tuberculosis drug, isoniazid with the citrate salt solutions using viscometric, acoustic, and spectroscopic techniques, J. Mol. Liq. 354 (2022), 118906.
[41] C. Yuan, B. Liu, H. Liu, Characterization of hydroxypropyl-β-cyclodextrins with different substitution patterns via FTIR, GC–MS, and TG–DTA, Carbohydr. Polym. 118 (2015) 36–40.
[42] Z.N. Abdulla, M.S. Hussein, Preparation of thiourea derivatives of isoniazid and evaluation of its bacterial activity, Mater. Today Proc. (2023). In press.
[43] N.A. Peppas, B. Narasimhan, Mathematical models in drug delivery: how modeling has shaped the way we design new drug delivery systems, J. Contr. Release 190 (2014) 75–81.